

RESEARCH ARTICLE

10.1002/2015JD024349

Key Points:

- A convection-permitting model run delivers the first annual cycle of haboobs over northern Africa
- A simple parameterization succeeds in reproducing the results in convection-parameterized model runs
- The parameterization has potential to solve a long-standing issue in simulating dust storms

Supporting Information:

- Figures S1–S7

Correspondence to:

F. Pantillon,
florian.pantillon@kit.edu

Citation:

Pantillon, F., P. Knippertz, J. H. Marsham, H.-J. Panitz, and I. Bischoff-Gauss (2016), Modeling haboob dust storms in large-scale weather and climate models, *J. Geophys. Res. Atmos.*, 121, 2090–2109, doi:10.1002/2015JD024349.

Received 16 OCT 2015

Accepted 8 FEB 2016

Accepted article online 11 FEB 2016

Published online 4 MAR 2016

Modeling haboob dust storms in large-scale weather and climate models

Florian Pantillon¹, Peter Knippertz¹, John H. Marsham², Hans-Jürgen Panitz¹, and Ingeborg Bischoff-Gauss³
¹Institute of Meteorology and Climate Research, Karlsruhe Institute of Technology, Karlsruhe, Germany, ²Water@Leeds, National Centre for Atmospheric Science, University of Leeds, Leeds, UK, ³Steinbuch Centre for Computing, Karlsruhe Institute of Technology, Karlsruhe, Germany

Abstract Recent field campaigns have shown that haboob dust storms, formed by convective cold pool outflows, contribute a significant fraction of dust uplift over the Sahara and Sahel in summer. However, in situ observations are sparse and haboobs are frequently concealed by clouds in satellite imagery. Furthermore, most large-scale weather and climate models lack haboobs, because they do not explicitly represent convection. Here a 1 year long model run with explicit representation of convection delivers the first full seasonal cycle of haboobs over northern Africa. Using conservative estimates, the model suggests that haboobs contribute one fifth of the annual dust-generating winds over northern Africa, one fourth between May and October, and one third over the western Sahel during this season. A simple parameterization of haboobs has recently been developed for models with parameterized convection, based on the downdraft mass flux of convection schemes. It is applied here to two model runs with different horizontal resolutions and assessed against the explicit run. The parameterization succeeds in capturing the geographical distribution of haboobs and their seasonal cycle over the Sahara and Sahel. It can be tuned to the different horizontal resolutions, and different formulations are discussed with respect to the frequency of extreme events. The results show that the parameterization is reliable and may solve a major and long-standing issue in simulating dust storms in large-scale weather and climate models.

1. Introduction

“Haboobs” [Sutton, 1925] are dust storms formed by the cold pool outflows from moist convective storms. Such storms vary in scale from hundreds of meters [Marsham *et al.*, 2009] to hundreds of kilometers [Roberts and Knippertz, 2014]. They are observed over most arid areas around the world and over the Sahel and Sahara in particular, which are the main sources of mineral dust worldwide (see Knippertz [2014] for a review). Recently, the first ever detailed in situ observations of meteorology and dust over the central Sahara showed that haboobs contribute at least half of dust emissions in summer [Marsham *et al.*, 2013a; Allen *et al.*, 2013, 2015]. Apart from this and earlier field campaigns over the fringes of the Sahara [Knippertz *et al.*, 2007; Flamant *et al.*, 2007; Bou Karam *et al.*, 2008; Marsham *et al.*, 2008; Marticorena *et al.*, 2010], detailed observations are rare in the region. Haboobs can hardly be distinguished in the sparse surface observations of meteorology and dust, and they are frequently concealed by clouds in satellite imagery [Heinold *et al.*, 2013; Kocha *et al.*, 2013]. Numerical modeling is therefore crucial to better understand the role of haboobs over the Sahara and in the global dust cycle. However, large-scale weather and climate models often lack haboobs, because they rely on parameterization schemes for subgrid convection that do not represent the cold pools and their propagation [Marsham *et al.*, 2011; Garcia-Carreras *et al.*, 2013; Heinold *et al.*, 2013; Largeron *et al.*, 2015; Sodemann *et al.*, 2015]. Statistical parameterizations of subgrid winds can improve the modeling of dust emissions at coarse resolution, but they are not able to represent haboobs [Ridley *et al.*, 2013].

To correct this major and long-standing limitation of large-scale dust models, Pantillon *et al.* [2015, hereafter PKMB15] suggested a simple parameterization of haboobs based on the downdraft mass flux of convection schemes. The parameterization of haboobs requires a model run with explicit convection for calibration. The available model data limited the results of PKMB15 to the western Sahel and Sahara and to the June–July 2006 period. Here an unprecedented model run with explicit convection over the whole of northern Africa and for the whole year of 2006 extends the original work of PKMB15 and offers new perspectives. The new model run allows estimating the seasonal cycle of haboobs and thus testing the parameterization over the

Table 1. List of Model Runs With Principal Characteristics of Their Configuration

Name	Grid spacing	Vertical levels	Moist convection	Domain
CTRL-P	0.44° (50 km)	35	Parameterized	Africa
HIRES-P	0.22° (25 km)	35	Parameterized	Africa
EXPL	0.025° (2.8 km)	50	Explicit	northern Africa

different parts of the Sahara, now including the eastern Sahel and Sahara as well as the Atlas Mountains. The parameterization is applied to two model runs with different horizontal resolutions, which further allows assessing its sensitivity. Different formulations of the parameterization are also discussed to better represent the intensity of haboobs.

Section 2 describes the configuration of the model runs, the estimate of dust-generating winds, the identification of haboobs, and the different formulations of the parameterization. Section 3 evaluates the representation of precipitation and dust-generating winds in the different runs, as compared to satellite and surface observations. Section 4 compares the distribution of explicit and parameterized haboobs in the different model runs and discusses the sensitivity to the model configuration as well as to the formulation of the parameterization. Finally, section 5 gives the conclusions of the paper and guides the use of the parameterization in large-scale weather and climate models.

2. Data and Methods

2.1. Model Runs

2.1.1. Configuration

This paper is based on 1 year long runs using the model of the Consortium for Small-Scale Modeling (COSMO) [Baldauf *et al.*, 2011] in Climate Mode (COSMO-CLM). COSMO-CLM is the community model of the German regional climate research. It was run over Africa for the year 2006 using ERA-Interim reanalyses [Dee *et al.*, 2011] as initial and lateral boundary conditions with the different configurations summarized in Table 1.

Based on the configuration of the Coordinated Regional climate Downscaling Experiment (CORDEX) [Panitz *et al.*, 2014], COSMO-CLM was run over the whole of Africa in a control run with parameterized convection (hereafter CTRL-P) with 0.44° (about 50 km) grid spacing and in a higher-resolution sensitivity run, also with parameterized convection (hereafter HIRES-P), with 0.22° (about 25 km) grid spacing, both with 35 terrain-following vertical levels. Both runs used the Tiedtke [1989] parameterization scheme for moist convection, which is based on a grid-scale moisture convergence closure. The model configuration was identical to that detailed in Panitz *et al.* [2014], except for a shorter time period and for additional model outputs of convective diagnostics.

In an unprecedented computational effort, COSMO-CLM was also run with 0.025° (about 2.8 km) grid spacing, which allows explicit representation of moist convection and thus of haboobs (hereafter EXPL). Following Gantner and Kalthoff [2010], the number of vertical levels was increased to 50 to better represent tropical deep convection. EXPL was run over a domain spanning almost all of Africa north of the equator (Figure 1). This domain was reduced compared to the other model runs due to high computational costs. Sensitivity runs with 0.44° grid spacing showed that increasing the domain size from northern Africa to the whole of Africa improved the timing of monsoon but did not significantly impact the results overall.

2.1.2. Verification

The Tropical Rainfall Measuring Mission (TRMM) product 3B42 [Huffman *et al.*, 2007] version 7, combining observations from several satellites and from rain gauges, is used to assess the modeled precipitation. It provides 3-hourly, spatially homogeneous observations on a 0.25° horizontal grid.

Surface synoptic observations (SYNOP) stations are used to assess the modeled wind. They provide 3-hourly observations of 10 m wind averaged over 10 min. Following Cowie *et al.* [2014], reported observations of wind speed above 55 knots (about 28 m s⁻¹) are considered spurious and thus excluded. SYNOP stations are sparse over northern Africa and over arid zones in particular (see their geographical distribution in Figure 7a). Moreover, the actual frequency of observations varies from region to region, e.g., with nighttime observations lacking over most of the Sahel (see Cowie *et al.* [2014] for a critical discussion of the quality of the SYNOP data over northern Africa). The observations must therefore be interpreted with caution.

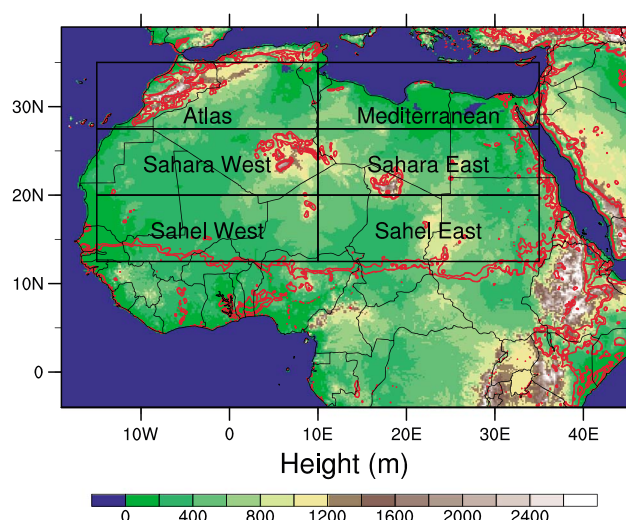


Figure 1. Domain and orography in the EXPL model run. Red contours show the roughness length at typical values of 0.05 and 0.1 m to mark the border between arid and vegetated areas. The areas defined in section 3 are marked by boxes and labeled.

2.1.3. Estimate of Dust-Generating Winds

Dust uplift depends on both atmospheric and soil controls. As the focus here is on the model representation of haboobs and not of dust sources, dust-generating winds are estimated with the dust uplift potential (DUP) [Marshall *et al.*, 2011]:

$$\text{DUP} = \nu U_{10}^3 \left(1 + \frac{U_t}{U_{10}} \right) \left(1 - \frac{U_t^2}{U_{10}^2} \right), \quad (1)$$

with ν the fraction of bare soil, U_{10} the 10 m wind speed, and U_t the threshold for dust uplift. DUP is based on the parameterization of Marticorena and Bergametti [1995] and isolates the atmospheric control; thus, dust uplift over a uniform surface is expected to depend on DUP only. A station- and season-dependent threshold U_t taken from Cowie *et al.* [2014] is used for the observed winds, while a space- and time-uniform threshold $U_t = 7 \text{ m s}^{-1}$ taken from Marshall *et al.* [2011] is used for the modeled winds in the absence of gridded values to use in the model. Although this gives a small mismatch in the thresholds between observations and model, Cowie *et al.* [2014] shows that it is the seasonal cycle in winds, not in thresholds, that determines the seasonal cycle in DUP.

2.1.4. Identification of Haboobs

Haboobs are detected in EXPL to tune the parameterization of haboobs in the other runs. Following Heinold *et al.* [2013], the leading edge of cold pools is automatically identified by thresholds for rapid cooling and strong updrafts. As in PKMB15, these thresholds are defined as -1 K h^{-1} on the anomaly in temperature tendency with respect to the mean diurnal cycle and 0.5 m s^{-1} on the vertical velocity, respectively. The temperature tendency is taken on the 925 hPa pressure level rather than at 2 m height, because the stable layer can prevent cold pools from reaching the surface at night [Heinold *et al.*, 2013]. The vertical velocity is taken on the 850 hPa pressure level, which shows a strong signal of updraft during cold pool propagation [e.g., Knippertz *et al.*, 2009; Roberts and Knippertz, 2014]. The surface wind is then attributed to a convective storm within 40 km of the identified leading edge of the cold pool. Although this automated identification largely matches a manual identification, it exhibits sensitivity to the chosen thresholds when the cold pools weakly contrast with their environment [Heinold *et al.*, 2013]. The chosen thresholds are rather conservative, and the identification therefore misses some of the haboobs. Sensitivity tests in PKMB15 suggests a relative uncertainty on the order of 30%.

2.2. Parameterization of Haboobs

2.2.1. Original Formulation

Haboobs are parameterized in the 0.44° and 0.22° runs following the conceptual model of PKMB15. The conceptual model is illustrated in Figure 2 and briefly described here. The downdraft mass flux

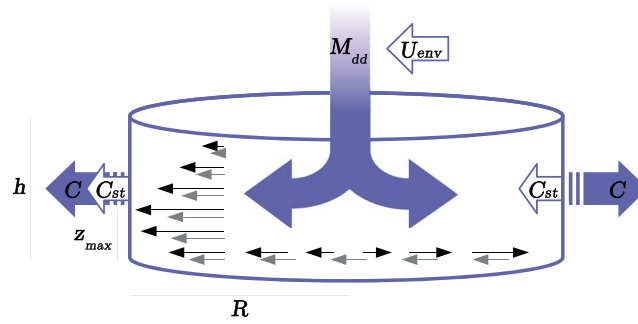


Figure 2. Schematic of the conceptual model, with M_{dd} the downdraft mass flux, U_{env} the environmental steering wind, C and C_{st} the propagation and steering speeds of the cold pool, respectively, h and R the height and radius of the cold pool, respectively, and z_{max} the height of maximum wind. Thin black and gray arrows illustrate the radial and the steering wind within the cold pool, respectively. From Pantillon et al. [2015]. ©American Meteorological Society. Used with permission.

from the convection scheme M_{dd} (kg s^{-1}) spreads out in a cylindrical cold pool that propagates radially with speed

$$C = \frac{M_{dd}}{2\pi R h \rho}, \quad (2)$$

with R the radius, h the height, and ρ the density of the cold pool. Within the cold pool, the wind speed increases linearly with increasing radius up to the leading edge R (black arrows in Figure 2), then decreases exponentially with radial length scale R_0 beyond R (not shown). The wind speed also increases logarithmically with increasing height up to the “nose” of the cold pool z_{max} , with a rate depending on the roughness length z_0 , then decreases linearly above z_{max} until it vanishes at height h (black arrows in Figure 2). The cold pool is further steered with speed $C_{st} = 0.65U_{env}$, with U_{env} the environmental wind at the height where M_{dd} originates from. Within the cold pool, the steering wind (gray arrows in Figure 2) follows the vertical profile of the radial wind (black arrows). The total wind is finally obtained as the vector addition of the radial and steering winds. For the sake of simplicity, the cold pool is considered static between two time steps. Here the parameterization of haboobs is applied offline to hourly model outputs, between which the cold pool is considered static. The conceptual model is thoroughly described in PKMB15.

The parameters of the conceptual model are tuned for the DUP from parameterized haboobs to match the DUP from haboobs identified in EXPL, on average over time and space. Based on an example of a developing cold pool in PKMB15, the parameters are set to $h = R/10$, $R_0 = R/3$, and $z_{max} = 100$ m. In the original formulation, the radius of cold pools R is taken as constant; thus, equation (2) becomes

$$C = \frac{5M_{dd}}{\pi R^2 \rho}, \quad (3)$$

and R is the only free parameter. As in PKMB15, M_{dd} from the Tiedtke [1989] scheme is further scaled with an arbitrary factor of 10 to reach realistic values.

2.2.2. Alternative Formulation

While the frequency of DUP from identified haboobs decreases quasi-logarithmically (blue curve in Figure 3), the frequency of DUP from parameterized haboobs is skewed, with quicker decrease for low DUP and slower decrease for high DUP in CTRL-P and HIRES-P (solid red and orange curves in Figure 3). In particular, the frequency of extreme DUP is overestimated. To reduce the skew, the surface area of the cold pool πR^2 is taken as proportional to the downdraft mass flux M_{dd} and the vertical velocity of downdrafts w_{dd} is taken as constant, i.e.,

$$M_{dd} = \pi R^2 \rho w_{dd}. \quad (4)$$

Equation (2) then becomes

$$C = 5w_{dd}; \quad (5)$$

thus, the propagation speed is constant and w_{dd} is the only free parameter. Note that M_{dd} still controls the integrated DUP through the surface area of the cold pool πR^2 in equation (4). The constant propagation speed

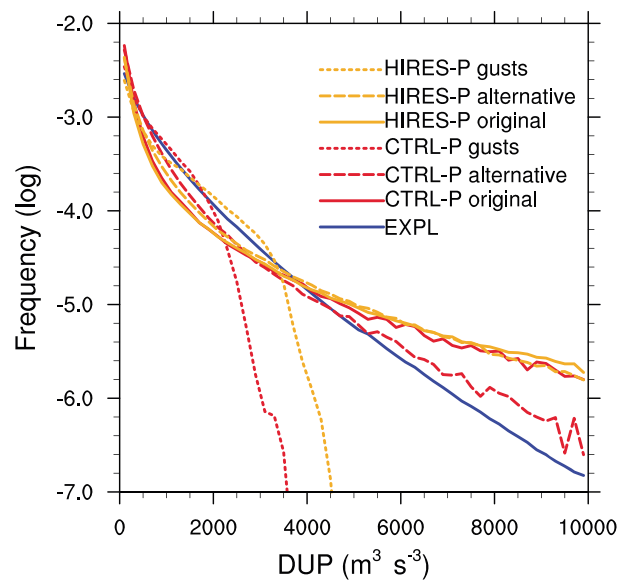


Figure 3. Probability distribution function of DUP computed over the year 2006 and over all domains displayed in Figure 11 from haboobs identified in EXPL and parameterized in CTRL-P and HIREs-P with the original, the alternative, and the gust formulations (Table 3).

of cold pools in the alternative formulation is typical of mesoscale convective systems [Houze, 2004], while the constant radius of cold pools in the original formulation is typical of downbursts [Fujita and Byers, 1977], both being observed sources of haboobs.

The alternative formulation successfully reduces the skew and the frequency of extreme DUP in CTRL-P (dashed red curve in Figure 3). However, the alternative formulation weakly impacts on the frequency of DUP in HIREs-P (dashed orange curve in Figure 3). Both formulations are therefore retained and compared in the rest of the paper. The parameterized DUP is further limited to $10^4 \text{ m}^3 \text{ s}^{-3}$ with both formulations to prevent too extreme events linked to very intense M_{dd} .

2.2.3. Gust Formulation

Following Nakamura *et al.* [1996], the maximum possible 10m wind speed from convective gusts $U_{10,conv}$ can be estimated from the downdraft convective available potential energy (DCAPE) and the horizontal momentum carried by a convective downdraft:

$$U_{10,conv} = \sqrt{\alpha \int_0^H 2g \frac{\theta_d - \theta}{\theta} dz + \beta U_H^2} \quad (6)$$

with H the height at which the downdraft starts, g the acceleration due to gravity, θ_d and θ the potential temperature of the downdraft and the environment, respectively, U_H the horizontal wind speed at height H , and α and β two tuning parameters. Although this formulation was originally suggested by Nakamura *et al.* [1996] for convective gusts in the midlatitudes, a similar formulation was suggested by Grandpeix and Lafore [2010] to parameterize the propagation speed of subgrid cold pools over Africa.

A parameterization of convective gusts using equation (6) is integrated in the Tiedtke [1989] scheme in COSMO, with the tuning parameter $\alpha = 0.2$ [Schulz and Heise, 2003]. The transport of horizontal momentum is not accounted for (i.e., $\beta = 0$) to avoid unrealistic strong gusts in cases of weak convection below a strong jet, and a threshold of 0.015 mmh^{-1} in convective precipitation is required to avoid too frequent gusts in light rain [Heise, 2006]. Here $U_{10,conv}$ was output without any threshold in convective precipitation, because the precipitation can evaporate before reaching the ground in haboobs over the Sahara. DUP is computed from $U_{10,conv}$ using equation (1) and scaled to match the DUP from identified haboobs on average over time and space. The scaling parameter σ represents the fractional surface of the grid cells over which convective gusts occur. The frequency of DUP with the gust formulation (dotted red and orange curves in Figure 3) matches that of identified dust storms at low DUP (blue curve in Figure 3) but drops at higher DUP and misses the tail of the distribution.

3. Evaluation of the Model Runs

The model runs are compared and assessed against available observations for precipitation and wind. The evaluation is focused on the arid and semiarid regions where haboobs occur. Six areas covering the same number of grid cells are defined and discussed in various parts of the paper (Figure 1): 27.5°N – 35°N and 15°W – 10°E (hereafter the Atlas, which also includes northern Algeria) or 10°E – 35°E (hereafter the Mediterranean); 20°N – 27.5°N and 15°W – 10°E (hereafter the Sahara west) or 10°E – 35°E (hereafter the Sahara east); and 12.5°N – 20°N and 15°W – 10°E (hereafter the Sahel west) or 10°E – 25°E (hereafter the Sahel east). Although haboobs also occur over the Arabian Peninsula, the evaluation is restricted to northern Africa.

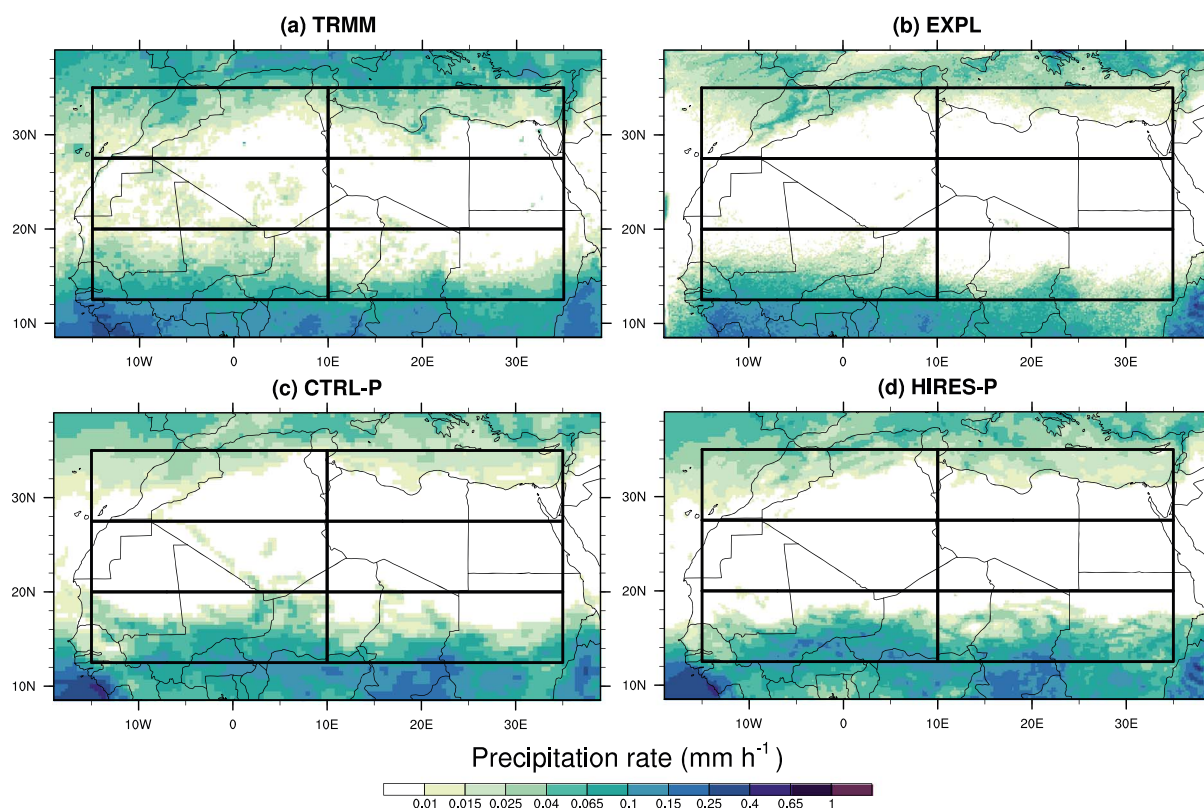


Figure 4. Spatial distribution of precipitation rate averaged over the year 2006 in the (a) TRMM-3B42 observation product and in the (b) EXPL, (c) CTRL-P, and (d) HIRES-P model runs (Table 1). The boxes mark the areas defined in section 3.

3.1. Precipitation

The observations exhibit three distinct regimes of precipitation (Figure 4a). The first is the tropical regime controlled by the monsoon over the Sahel west and east. The second is the subtropical regime over the Atlas and Mediterranean, with precipitation concentrating on the mountains and on the sea. The third is the dry regime with very weak precipitation over the Sahara west and east. These regimes show different seasonal cycles. The precipitation reaches a strong peak in August over the Sahel west and east (black curves in Figures 5e and 5f) due to the maximal northward extension of the monsoon. The precipitation reaches a weaker peak in January over the Atlas and Mediterranean (black curves in Figures 5a and 5b) due to the maximal activity of midlatitude systems. The precipitation finally exhibits both peaks but with weaker amplitude over the Sahara west and east (black curves in Figures 5c and 5d).

The model runs differ in their representation of the monsoon. The EXPL run captures the northward extension (Figure 4b) as well as the timing but underestimates the amplitude compared to the observations (blue curves in Figures 5e and 5f). The CTRL-P and HIRES-P runs also capture the northward extension of the monsoon (Figures 4c and 4d) and better capture the amplitude but exhibit too early onset and too late retreat (red and orange curves in Figures 5e and 5f).

The model runs agree better in the representation of the subtropical regime, as they all underestimate the observed precipitation in fall and winter over the Atlas and Mediterranean (Figures 5a and 5b). This suggests that the model resolution plays a minor role in the representation of the subtropical compared to the tropical regime. The model runs differ again in the representation of the dry regime over the Sahara west and east, where EXPL and HIRES-P lack any precipitation whereas CTRL-P exhibits tracks of individual systems (Figures 4b–4d, 5c, and 5d).

The observations exhibit a clear diurnal cycle of precipitation (black curve in Figure 6). They reach a peak in the afternoon when convection is triggered, then decrease slowly in the evening when organized convective

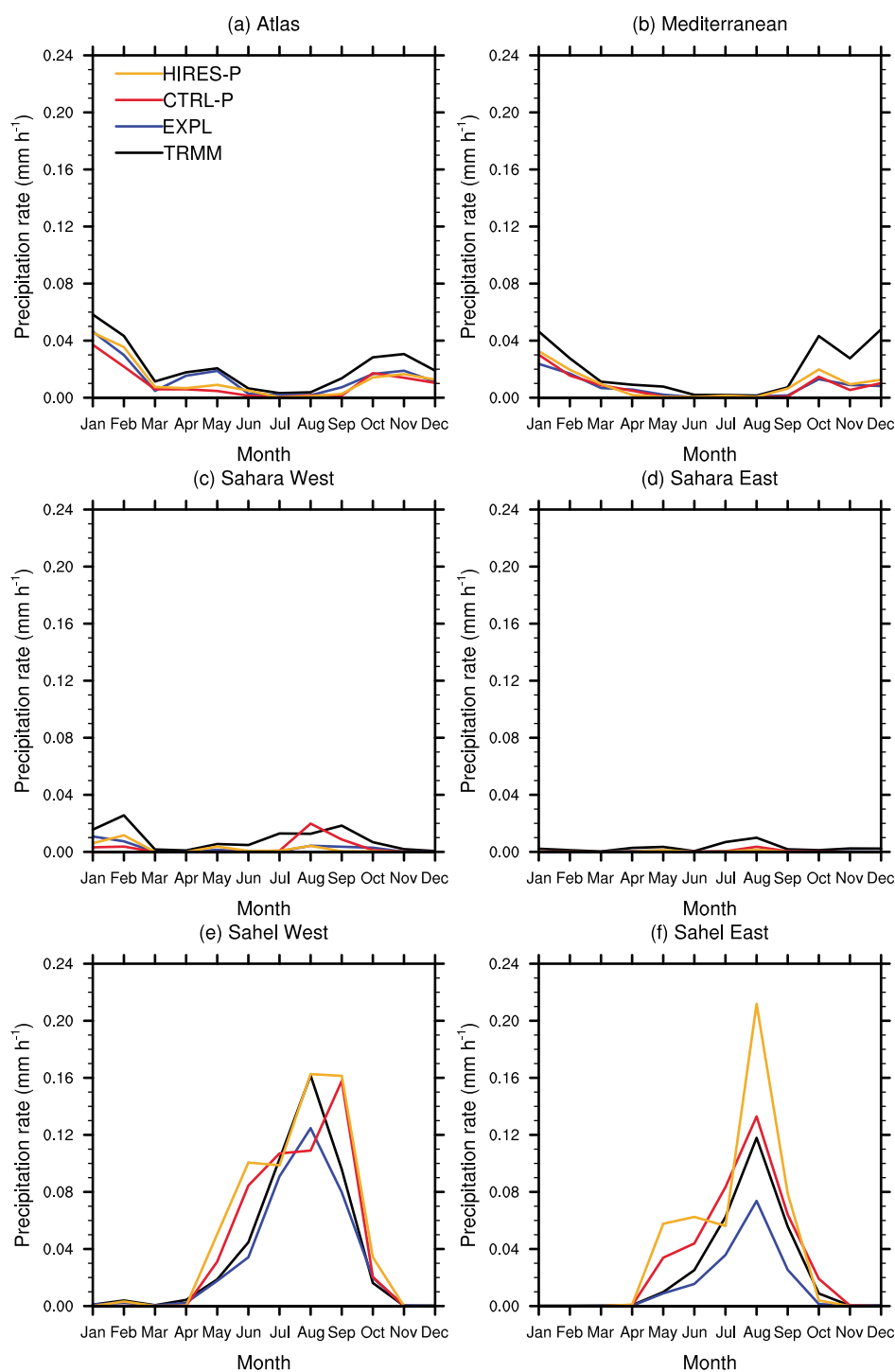


Figure 5. Seasonal cycle in precipitation rate averaged over each area marked by a box in Figure 4 in the TRMM-3B42 observation product and in the EXPL, CTRL-P, and HIRE5-P model runs (Table 1).

systems propagate, and decrease quicker in the morning when the systems disaggregate. This diurnal cycle is mainly influenced by the tropical regime, since the diurnal cycle exhibits a smaller amplitude in the subtropical and dry regimes (see supporting information Figure S1 for the diurnal cycle of precipitation over each area). Note that the area-averaged diurnal cycle in Figure 6 is a composite of local diurnal cycles that strongly vary geographically, as organized convective systems tend to form over mountain ranges and propagate to the west [Fink and Reiner, 2003; Laing et al., 2008].

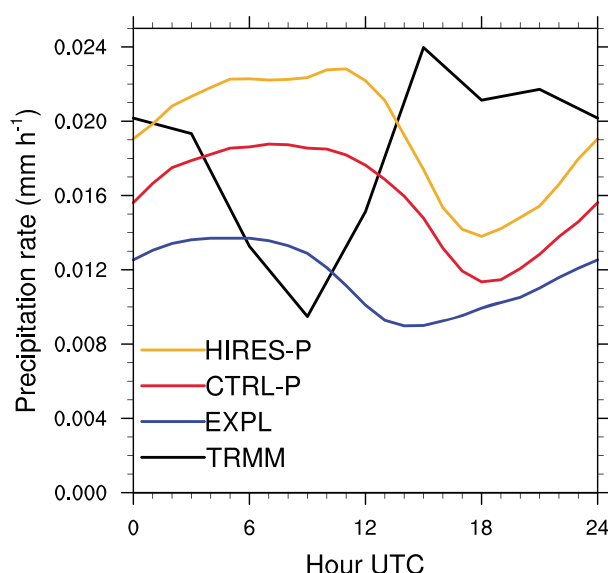


Figure 6. Diurnal cycle in precipitation rate averaged over the year 2006 and over all areas marked by boxes in Figure 4 in the TRMM-3B42 observation product and in the EXPL, CTRL-P, and HIRES-P model runs (Table 1).

The model runs strongly contrast with the observations and exhibit a surprisingly similar diurnal cycle of precipitation considering their different representation of convection. The EXPL run exhibits a diurnal cycle of weak amplitude, where precipitation slowly increases in the afternoon and evening to peak at night (blue curve in Figure 6). The delay compared to the observations (black curve in Figure 6) suggests that the lifetime of organized convective systems is overestimated in EXPL (V. Maurer, manuscript in preparation, 2016). The CTRL-P and HIRES-P runs peak at noon (red and orange curves in Figure 6), which is expected with parameterized convection. However, the precipitation also increases in the evening and at night. The modeled diurnal cycles in Figure 6 are also influenced by the tropical regime mainly but are found in the other regimes as well, albeit with smaller amplitude (see Figure S1 for the diurnal cycle of precipitation over each area).

3.2. Dust Uplift Potential

The density of the SYNOP network drops over arid zones; thus, some single stations are crucial to capture the relevant processes for dust emission. In particular, the station of Faya in northern Chad exhibits the highest observed DUP (18°N, 19°E in Figure 7a). Faya is located in the Bodélé Depression, which is known as a major source of dust due to the strong low-level jet in winter and spring [Washington and Todd, 2005]. The station of Bordj Badji Mokhtar in southern Algeria also exhibits high observed DUP (21°N, 1°E in Figure 7a). Bordj Badji Mokhtar is located close to the center of the Saharan heat low in summer, which is also a major source of dust [Marshall et al., 2013a; Allen et al., 2013, 2015]. Further stations exhibit high DUP over northeastern Sudan and over central Algeria, as well as near the Atlantic and Mediterranean coasts. In contrast, the stations exhibit lower DUP over the western Sahel and over the Libyan Desert (Figure 7a).

The model runs capture the observed pattern of DUP overall but differ regionally. They succeed in exhibiting highest DUP over the Bodélé Depression around Faya, high DUP over central Algeria and near the Atlantic and Mediterranean coasts, and low DUP over the Libyan Desert (Figures 7b–7d). In contrast, the model runs locally fail in exhibiting high DUP, e.g., over the southern Sahara around Bordj Badji Mokhtar. The model runs furthermore overestimate DUP over the western Sahel, where the match between the sharp meridional gradient in modeled DUP and in roughness length (contours in Figure 1) suggests a too low roughness length in the model (see also Figure S2 for a scatterplot of DUP between observations and EXPL subsampled at SYNOP stations). Beyond the geographical pattern, the magnitude of DUP increases with increasing model resolution (Figures 7b–7d), in particular over mountain ranges (contours).

The observed and modeled DUP are further compared with respect to their seasonal and diurnal cycles. The observed DUP is aggregated over each area and scaled with the fraction of land for comparison with the modeled DUP. Although the comparison is affected by the density of stations and the frequency of observations, results are consistent with subsampling the modeled wind to the location and time of observations (see Figure S3 for the correlation of seasonal and diurnal cycles of DUP between observations and EXPL subsampled at SYNOP stations). As dust uplift is unlikely on elevated ground, elevations over 800m are excluded from the modeled DUP. They are, however, included in the observed DUP, because only four SYNOP stations are concerned. Among them is the crucial station of Bordj Badji Mokhtar, which is located at 816m above sea level but of which the elevation remains below 800m in the model orography (contours in Figures 7b–7d).

The observed DUP reaches a strong seasonal peak in winter over the Sahel east (black curve in Figure 8f) due to the contribution of the strong low-level jet, in Faya in particular. It also reaches a seasonal peak in winter

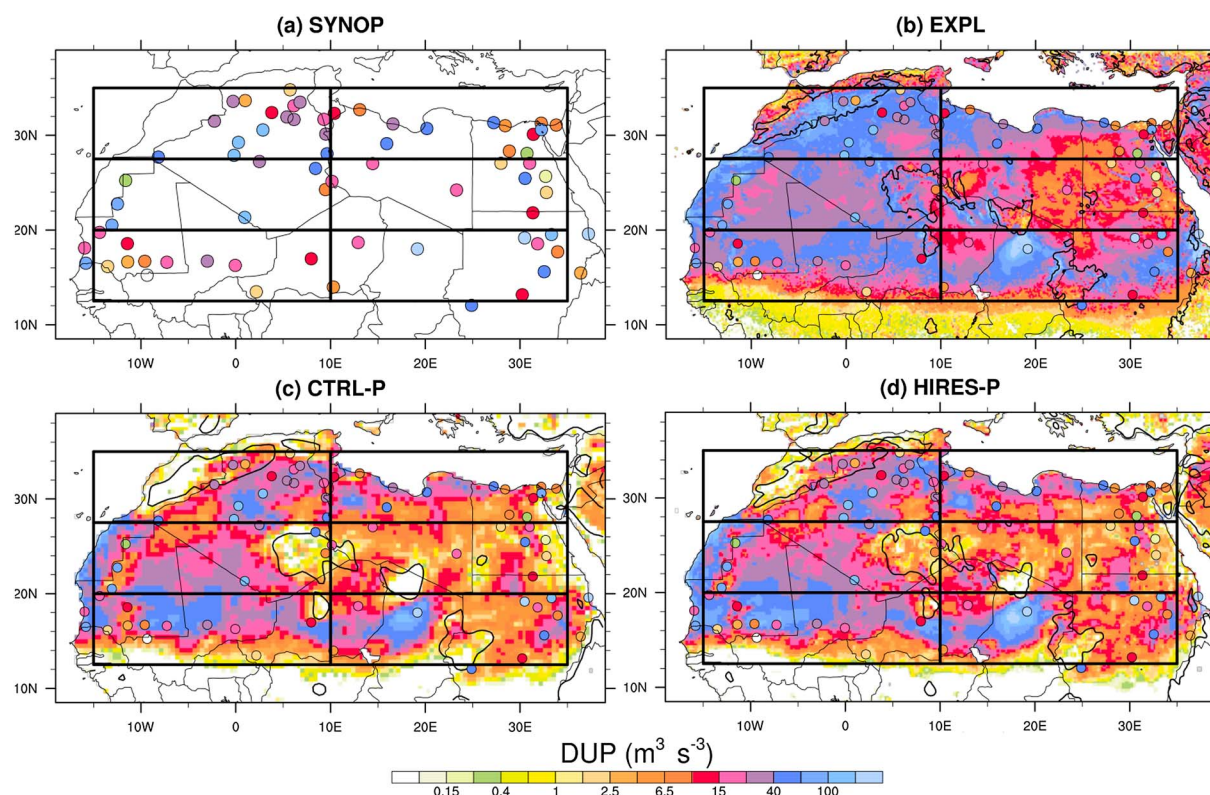


Figure 7. Spatial distribution of DUP averaged over the year 2006 (a) from the observed wind at SYNOP stations and from the resolved model wind in the (b) EXPL, (c) CTRL-P, and (d) HIRES-P model runs (Table 1). The DUP in Figure 7a is overplotted in Figures 7b–7d for comparison. The contours in Figures 7b–7d show the 800m elevation in the model runs. The boxes mark the areas defined in section 3.

over the Atlas and Mediterranean (black curves in Figures 8a and 8b) due to midlatitude systems such as lee cyclones over the Atlas and Sharav cyclones [Alpert and Ziv, 1989] over the Mediterranean. In contrast, the observed DUP reaches a seasonal peak in summer over the Sahara west (black curve in Figure 8c), which matches the monsoon cycle (Figure 5c). Finally, the observed DUP exhibits a rather flat seasonal cycle over the Sahara east and Sahel west (Figures 8d and 8e). In the diurnal cycle, the observed DUP reaches a peak in the morning (black curve in Figure 9) due to the downbreak of the nocturnal low-level jet [Fiedler et al., 2013], then slowly decreases in the afternoon due to dry convection in the boundary layer [Parker et al., 2005] and remains low at night due to the stable layer inhibiting strong surface winds (see Figure S4 for the diurnal cycle of DUP over each area).

The model runs capture the observed morning peak and its slow decrease in the diurnal cycle of DUP, although delayed, and again with magnitude depending on the model resolution (Figure 9). However, the model runs lack the observed winter peak in the seasonal cycle of DUP over the Sahel east (Figure 8f), which suggests that they underestimate the contribution of the low-level jet (see Fiedler et al. [2013] for a discussion of the representation of the nocturnal low-level jet and its breakdown in models). The model runs also lack the observed winter peak over the Atlas and Mediterranean (Figures 8a and 8b), which suggests that they underestimate the contribution of midlatitude systems to DUP. The model runs better match the observations over the Sahara west, where they reach a seasonal peak in summer (Figure 8c). The model runs also reach a seasonal peak in summer over the Sahel west (Figure 8e), which strongly overestimates the observed DUP and again suggests a too low roughness length in the model (contours in Figure 1).

3.3. Discussion

The strong circulation of the Saharan heat low, as well as monsoon surges, contribute to the summer peak in DUP over the Sahara west (Figure 8c). In addition, further processes also contribute to the summer peak in modeled DUP. Mesoscale convective systems produce strong surface winds at the leading edge of cold pools (Figure 10a). Although they are driven by moist convection, they generally do not produce surface precipitation over the Sahara, where the evaporation is too strong. Mesoscale convective systems are found in EXPL

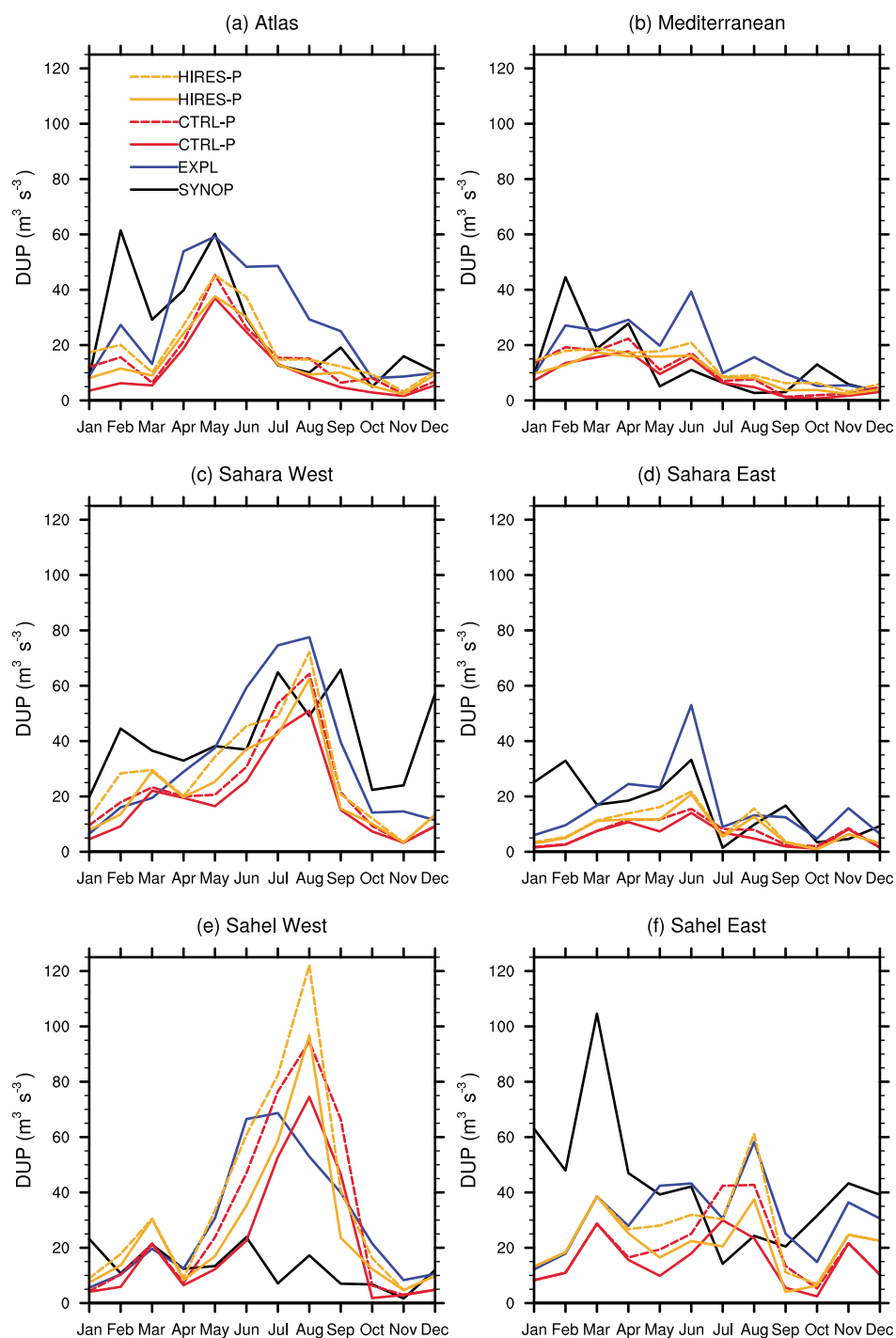


Figure 8. Seasonal cycle in DUP averaged over each area marked by a box in Figure 7 from the observed wind at SYNOP stations and from the resolved model wind in the EXPL, CTRL-P, and HIRES-P model runs (Table 1). The dashed curves show the total DUP from the resolved model wind and the haboobs parameterized with the original formulation.

only, because their formation and propagation require the explicit representation of convection [Marshall *et al.*, 2011; Garcia-Carreras *et al.*, 2013; Heinold *et al.*, 2013; Largeron *et al.*, 2015; Sodemann *et al.*, 2015].

The parameterized runs also exhibit some organization of convection but mostly with weak surface winds. However, cases of extreme surface winds created by deep cyclones are found in CTRL-P and HIRES-P (Figure 10b). The deep cyclones form in August and September over the Sahel and migrate westward then

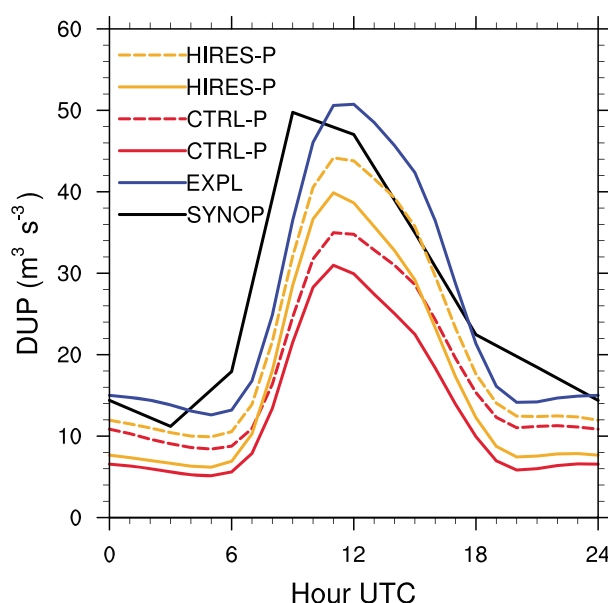


Figure 9. Diurnal cycle in DUP averaged over the year 2006 and over all areas marked by boxes in Figure 7 from the observed wind at SYNOP stations and from the resolved model wind in the EXPL, CTRL-P, and HIRES-P model runs (Table 1). The dashed curves show the total DUP from the resolved model wind and the haboobs parameterized with the original formulation.

northwestward into the Sahara. The single case illustrated here contributes most of the September DUP over the Sahel west and Sahara west in CTRL-P. A few of such cyclones are also responsible for the precipitation over the Sahara west in CTRL-P (Figure 4c) and for the peak in September over the Sahel west in CTRL-P and HIRES-P (Figure 5e).

At first sight, the modeled deep cyclones match the concept of Soudano-Saharan depressions, whose exact definition and meteorological characteristics are somewhat unclear [Schepanski and Knippertz, 2011]. They also exhibit similarities with tropical cyclones, which can form in August and September from African easterly waves but exclusively offshore [e.g., Berry and Thorncroft, 2005]. We therefore suggest that the deep cyclones are a model artifact and are due to the failure of the convective parameterization in releasing the atmospheric instability through mesoscale convective systems.

The convective parameterization contributes little to the precipitation associated with the deep cyclones, which thus only weakly affect the parameterization of haboobs.

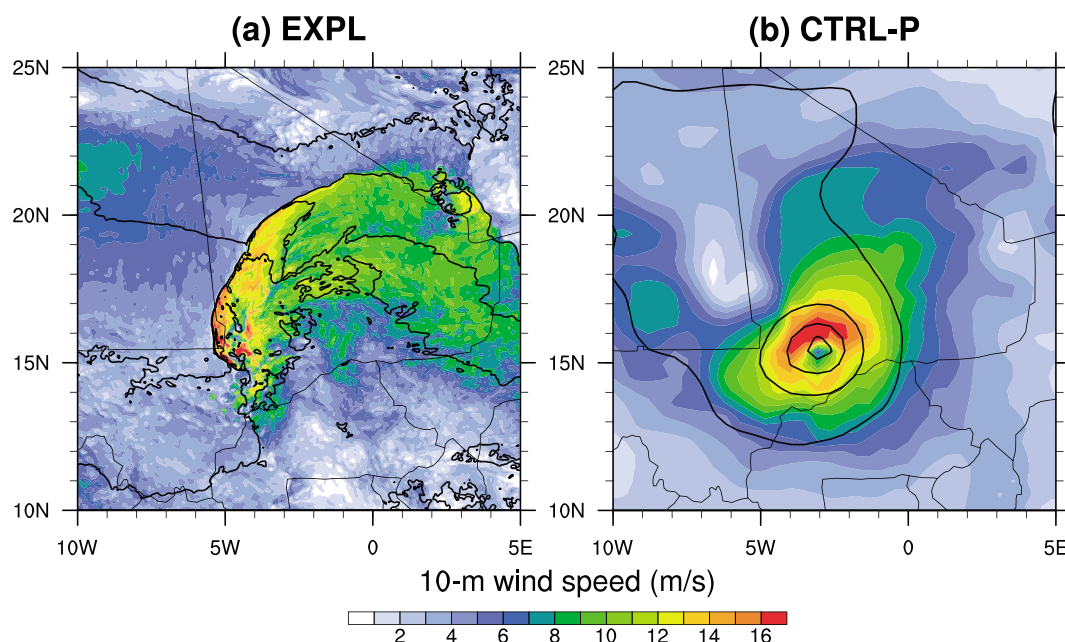


Figure 10. Examples of storms in the model runs: (a) mesoscale convective system at 1800 UTC on 3 August 2006 in EXPL and (b) deep cyclone at 0600 UTC on 10 September 2006 in CTRL-P. Contours show the 925 hPa temperature every 5 K in Figure 10a and the mean sea level pressure every 5 hPa in Figure 10b.

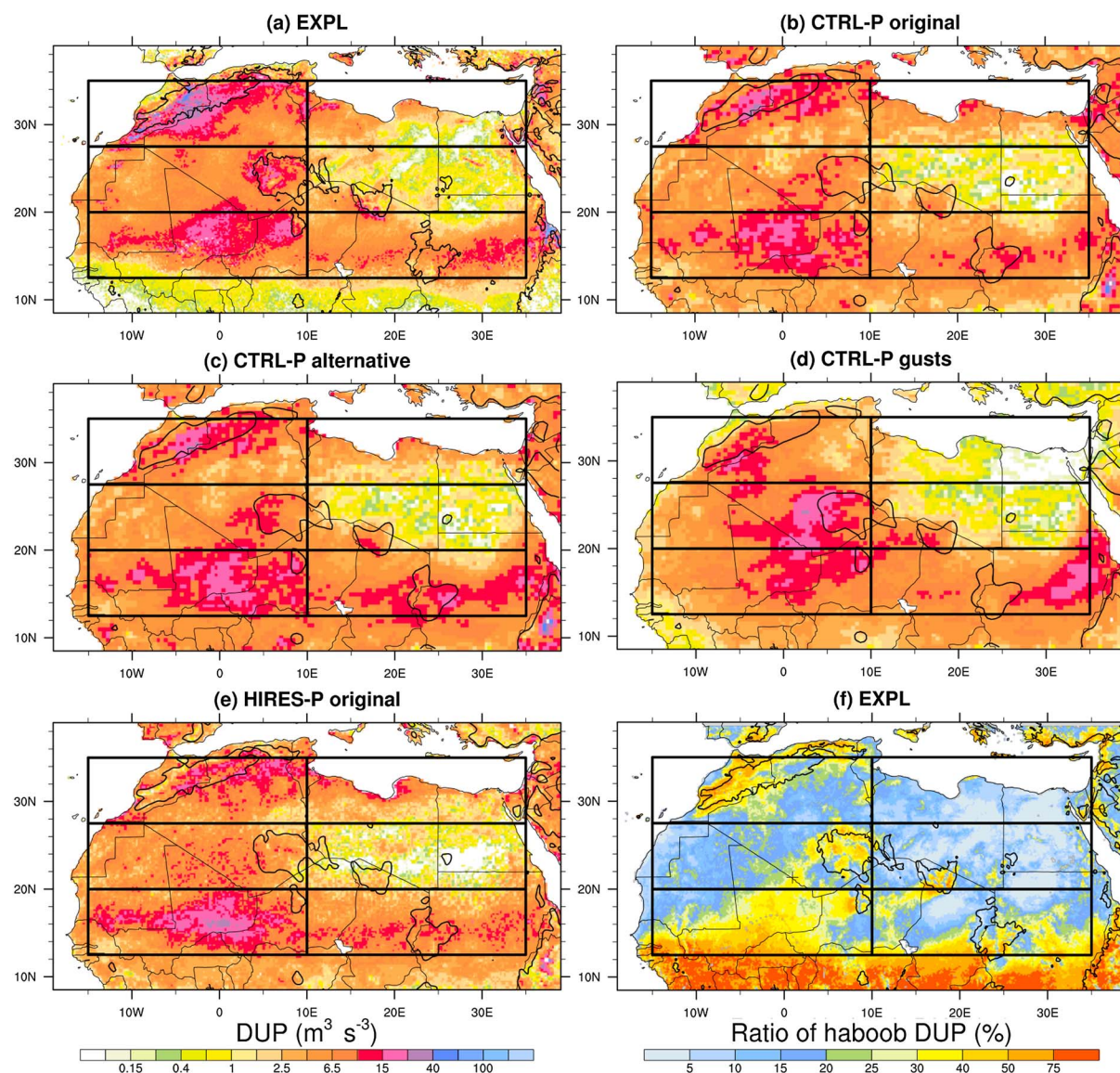


Figure 11. Spatial distribution of DUP averaged over the year 2006 from haboobs (a) identified in EXPL, (b) parameterized in CTRL-P with the original formulation, (c) the alternative formulation, and (d) the gust formulation, and (e) parameterized in HIRES-P with the original formulation, and (f) ratio of haboob to total DUP in EXPL. The boxes mark the areas defined in section 3. The plus symbol in Figure 11f marks the position of Bordj Badji Mokhtar.

4. Haboobs in the Model Runs

The spatial distribution and seasonal and diurnal cycles of haboobs are given here for the different model runs. The identified haboobs are first discussed in the EXPL run and compared to those observed during field campaigns. The parameterized haboobs are then discussed for the CTRL-P and HIRES-P runs, using the different formulations of the parameterization, and compared to those identified in EXPL.

4.1. Explicit Haboobs

The EXPL run exhibits high DUP from haboobs in relation with both orographic convection and the monsoon flow. Highest DUP is found in the Atlas area, over the mountain range itself and over the southern foothills (Figure 11a). High DUP is also found over a wide region in the Sahel west area, over the Hoggar Mountains in the Sahara west, and over Sudan in the Sahel east area. In contrast, low DUP is found in the dry Sahara east and Mediterranean areas, as well as over the southern part of the Sahel west area. As in the DUP from the model's total wind (Figure 7), a sharp meridional gradient over the Sahel west (Figure 11a) matches that in roughness length (contours in Figure 1).

Table 2. DUP Attributed to Haboobs in the Explicit Run, Averaged Over the Whole Year 2006 and Over the May–October Period Only, in $\text{m}^3 \text{s}^{-3}$ and as Fraction of the Total DUP in Brackets

	Atlas	Mediterranean	Sahara West	Sahara East	Sahel West	Sahel East	All
Whole year	6.1 (21%)	1.7 (10%)	5.6 (17%)	1.5 (9%)	8.0 (28%)	5.0 (16%)	4.6 (18%)
May–October	9.2 (25%)	1.9 (12%)	10.3 (21%)	2.0 (11%)	15.3 (33%)	9.7 (27%)	8.1 (24%)

To some extent, the pattern of DUP from haboobs (Figure 11a) matches the pattern of total DUP (Figure 7b), with high DUP over the Atlas and the Sahel west and low DUP over the Sahara east. The contribution of haboobs to the total DUP, however, contrasts between the areas and is generally higher where the total DUP is higher (Figure 11f). It reaches 28% over the Sahel west but 9% only over the Sahara east and 18% on average over all areas (Table 2). The contribution of haboobs is higher during the May–October period, when it reaches 24% on average and up to 33% over the Sahel west. As in the seasonal and diurnal cycles, elevations below 800m only are considered here.

Haboobs exhibit a strong seasonal cycle in EXPL, with high activity in spring and summer in the different areas. In the Atlas area, DUP reaches a primary peak in May and a secondary peak in July (blue curve in Figure 12a). Haboobs in the area are related to upper level troughs from the midlatitudes, which reduce the atmospheric stability and favor convection [Knippertz *et al.*, 2007]. The low DUP in the Mediterranean and Sahara east areas exhibits similar seasonal cycles but with much smaller amplitudes (blue curves in Figures 12b and 12d). Over the Sahel west and east and the Sahara west, the seasonal cycle is controlled by the monsoon. DUP in the Sahel west quickly increases in May to reach a primary peak in June during the monsoon onset, then reaches a secondary peak in August during the monsoon maximum before quickly decreasing in September during the monsoon retreat (blue curve in Figure 12e). The August peak has larger amplitude than the June peak in the Sahara west and Sahel east areas, where the monsoon flow arrives later in the season (blue curves in Figures 12c and 12f). The different areas exhibit similar diurnal cycles of DUP, which increases in the afternoon to reach a peak or a plateau in the evening, then decreases at night (blue curve in Figure 13; see Figure S5 for the diurnal cycle of haboobs over each area).

These results are consistent with the available observations of haboobs, although the modeled DUP and the observed frequency of storms are different diagnostics and thus can be compared qualitatively only. Several haboobs were observed in May–June 2006 over southern Morocco during the Saharan Mineral Dust Experiment (SAMUM) field campaign [Knippertz *et al.*, 2007]. Frequent cold pools from moist convection were further observed over the area in May–September during the 2002–2006 period [Emmel *et al.*, 2010] at surface stations of the Integrated Approach to the Efficient Management of Scarce Water Resources in West Africa (IMPETUS) project. The highest activity was observed in August and attributed to the midlevel transport of moisture from the Sahel [Knippertz *et al.*, 2003; Knippertz, 2003]. These results were confirmed when the study was extended to the 2002–2012 period and to northern Algeria and Tunisia [Redl *et al.*, 2015]. They validate the high DUP found over the Atlas in EXPL (Figure 11a). The relatively low modeled activity in August (blue curve in Figure 12a) may be due to a lack of moisture transport from the Sahel in the model or to a lower activity in August 2006 compared to other years.

Over the Sahel west, haboobs were observed in June 2006 during the African Monsoon Multidisciplinary Analysis (AMMA) field campaign [Flamant *et al.*, 2007; Bou Karam *et al.*, 2008]. Intense haboobs were further observed over the area from the end of May to the end of July during the 2006–2008 period at the AMMA Sahelian Dust Transect of three stations aligned around 14°N [Marticorena *et al.*, 2010]. The majority of the haboobs were observed in the evening, which is consistent with high evening DUP in EXPL (blue curve in Figure 13). These results also validate the primary peak in modeled DUP in June (blue curve in Figure 12e). The secondary peak in modeled DUP in August suggests a too weak seasonal cycle of roughness length in the model.

To the best of the authors' knowledge, haboobs were not documented over the other areas in 2006; thus, the modeled DUP is assessed against observations from other years. Over the Sahara west, haboobs were observed at Bordj Badji Mokhtar in June 2011 and 2012, at night mostly, and contributed 50–70% of dust emissions [Marshall *et al.*, 2013a; Allen *et al.*, 2013, 2015]. This is consistent with the secondary peak in modeled DUP in June (blue curve in Figure 12c), with the higher modeled DUP between 18 and 06 UTC

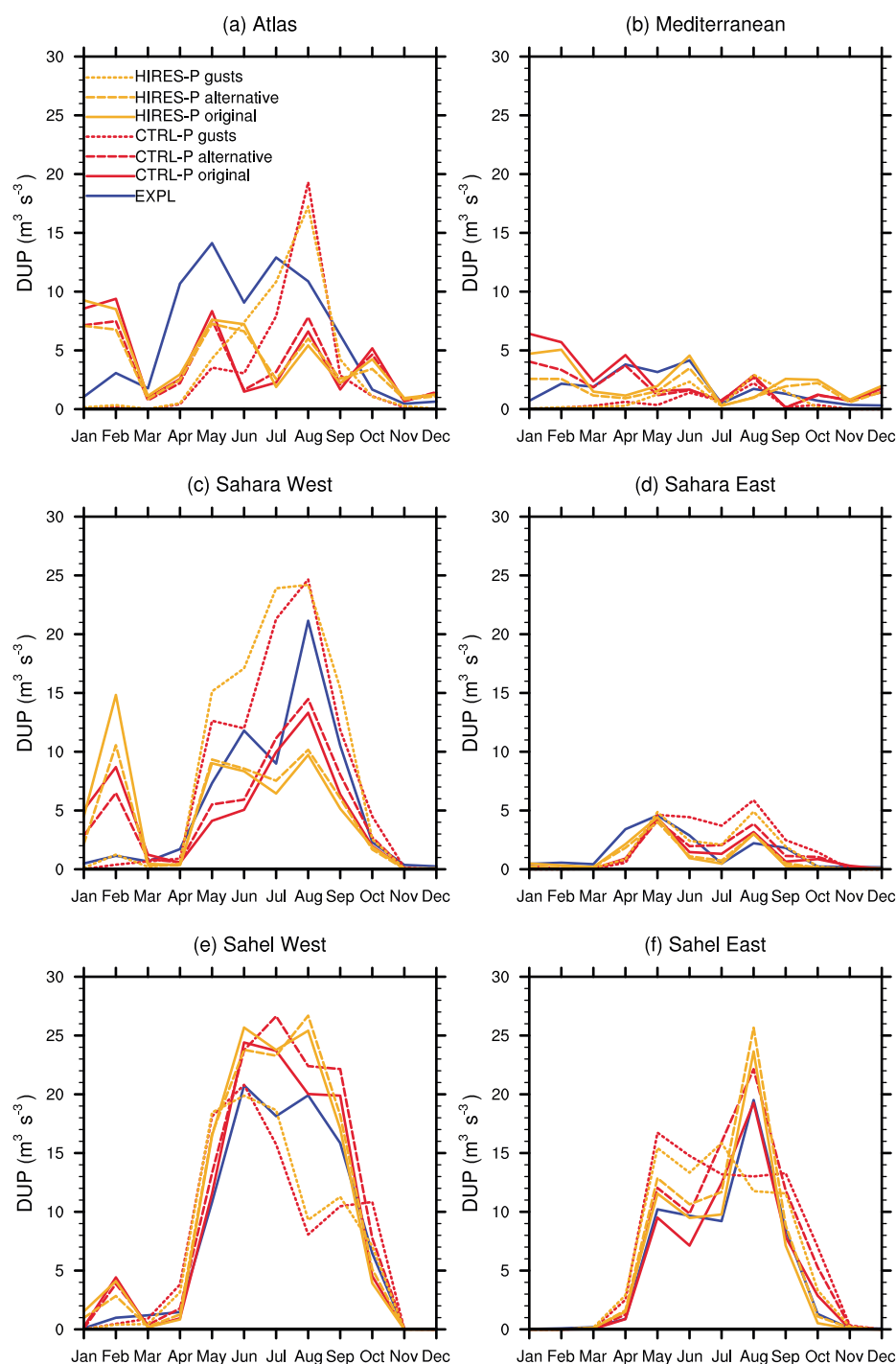


Figure 12. Seasonal cycle in DUP averaged over each area marked by a box in Figure 11 from haboobs identified in EXPL and parameterized in CTRL-P and Hires-P with the original, the alternative, and the gust formulations (Table 3).

(blue curve in Figure 13), and with the area of high haboob-to-total DUP ratio extending to Bordj Badji Mokhtar (plus symbol in Figure 11f).

In contrast with Bordj Badji Mokhtar, few haboobs were observed at Zouerate, northern Mauritania, in June 2011 [Todd et al., 2013], which is also consistent with the lower modeled DUP over that region (Figure 11a). Over the Sahel east, the first climatology of haboobs reported cases over Khartoum between May and October and highest activity in June [Sutton, 1925]. This agrees with the modeled activity from May to September but

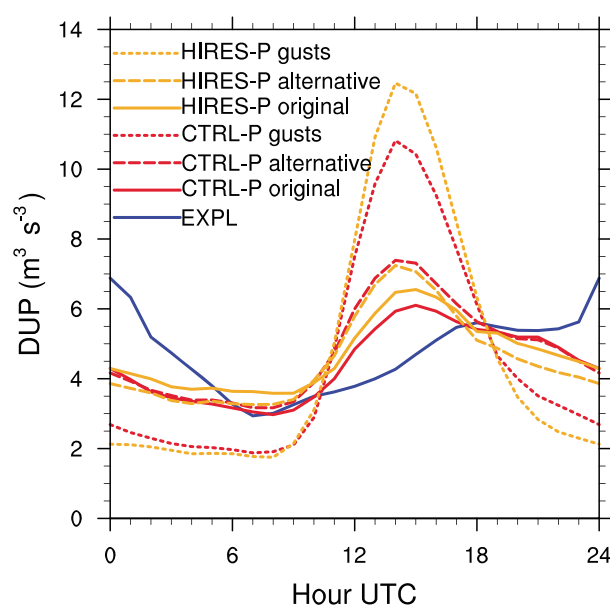


Figure 13. Diurnal cycle in DUP averaged over the year 2006 and over all areas marked by boxes in Figure 11 from haboobs identified in EXPL and parameterized in CTRL-P and HIRES-P with the original, the alternative, and the gust formulations (Table 3).

contrasts with the modeled peak in August (blue curve in Figure 12f). This also suggests a too weak seasonal cycle of roughness length in the model, although the 1916–1923 period documented by Sutton [1925] may not be comparable to 2006. Finally, the low DUP over the Sahara east and the Mediterranean areas (blue curves in Figures 12b and 12d) is consistent with the extreme dryness of the Libyan Desert [e.g., O'Hara *et al.*, 2006] and thus the lack of moist convective storms.

The modeled DUP in EXPL can also be compared to the modeled DUP in the run with explicit convection used in PKMB15. This run was performed with the UK Met Office Unified Model [Walters *et al.*, 2011] using a 4 km grid spacing over the western Sahel and Sahara for the June–July 2006 period (hereafter the 4 km run). The EXPL and 4 km runs agree on the high DUP from haboobs over northern Mali, while high DUP over the Hoggar and Air Mountains is found in EXPL only (compare Figure 11a here with Figure

11a in PKMB15), which suggests stronger orographic convection in EXPL than in the 4 km run. The two runs differ in the location of the sharp meridional gradient in DUP, which is again closely related to the pattern of roughness length (compare the contours in Figure 1 with Figure 1c in PKMB15). Despite the differences in the spatial distribution, the two runs compare well in the contribution of haboobs to the total DUP, with 16% in the 4 km run (PKMB15) and 22% in EXPL over the same area and time period. The spatial distribution in EXPL is weakly impacted by considering the whole year instead of the June–July period only (compare Figure S6 with Figure 11a).

However, the diurnal cycle differs markedly between the two runs, as the 4 km run exhibits a strong and narrow peak at 18 UTC (Figure 12 in PKMB15), while EXPL exhibits a weak and broad peak between 18 and 00 UTC (blue curve in Figure 13). A weak and broad peak at 00 UTC is also found in EXPL over the western Sahel and Sahara for the June–July period only as in PKMB15 (Figure S7). The difference in diurnal cycle of DUP is consistent with the difference in the diurnal cycle of precipitation, which exhibits a too strong and narrow peak in the 4 km run [Marshall *et al.*, 2013b; Birch *et al.*, 2014] and a too weak and broad peak in EXPL (blue curve in Figure 6) as compared to TRMM observations. This suggests that haboobs are too short lived in the 4 km run and too long lived in EXPL.

4.2. Parameterized Haboobs

The parameterization of haboobs in CTRL-P and HIRES-P is tuned to match the DUP averaged over the whole year 2006 and over all areas in EXPL, excluding elevations over 800m. The root-mean-square error (RMSE) of

Table 3. Tuning of the Parameterization for Each Run and Formulation, and Spatial and Seasonal Root-Mean-Square Error (RMSE) of DUP (in $\text{m}^3 \text{s}^{-3}$) With Respect to EXPL

Run	Formulation	Tuning	Spatial RMSE	Seasonal RMSE
CTRL-P	Original	$R = 6.0 \text{ km}$	3.39	3.26
CTRL-P	Alternative	$w_{dd} = 5.0 \text{ m s}^{-1}$	3.42	3.17
CTRL-P	Gusts	$\sigma = 0.09$	3.81	3.87
HIRES-P	Original	$R = 3.5 \text{ km}$	3.56	3.60
HIRES-P	Alternative	$w_{dd} = 5.4 \text{ m s}^{-1}$	3.57	3.20
HIRES-P	Gusts	$\sigma = 0.12$	3.88	3.78

the parameterization is also computed with respect to EXPL (Table 3). The spatial RMSE is first computed from the annual DUP interpolated on the 0.44° grid then averaged over all areas, while the seasonal RMSE is first computed from the monthly DUP over each area then averaged over all months and all areas.

The different runs require different tuning parameters. With the original formulation, the tuning parameter R approximately scales with the grid spacing between CTRL-P and HIRES-P (Table 3). In equation (3), this compensates for M_{dd} approximately scaling with the grid surface area, i.e., the square of the grid spacing. With the alternative formulation, the tuning parameter w_{dd} weakly changes with the grid spacing between CTRL-P and HIRES-P (Table 3). This is due to C not depending on M_{dd} in equation (5). Finally, with the gust formulation (equation (6)), the tuning parameter σ increases between CTRL-P and HIRES-P (Table 3), which compensates for DCAPE decreasing with grid spacing.

The parameterization captures the geographical pattern of identified haboobs in EXPL (Figure 11a) but with some sensitivity to the model run and to the formulation. When applied to CTRL-P with the original formulation, the parameterization succeeds in exhibiting highest DUP over the Atlas area, high DUP over a wide region in the Sahel west area, and low DUP over the Sahara east (Figure 11b). The parameterization, however, misses local features of DUP and lacks the sharp meridional gradient in the southern part of the Sahel west area. Using the alternative formulation weakly affects the spatial distribution of parameterized DUP, with differences in local features only (Figure 11c). In contrast, using the gust formulation strongly impacts on the spatial distribution. The large region of high DUP is shifted from the Sahel west to the Sahara west, and the region of low DUP is extended from the Sahara east to the Mediterranean (Figure 11d). This suggests that computing the DCAPE in the deep Saharan boundary layer overestimates the parameterized DUP. The northward shift in DUP increases the spatial RMSE as compared to the original and alternative formulations, which perform equally well (Table 3).

Applying the parameterization to HIRES-P instead of CTRL-P produces smaller-scale features, as expected from the higher resolution, but weakly affects the spatial distribution, either with the original formulation (Figure 11e) or with the alternative and the gust formulations (not shown). The spatial RMSE slightly increases in HIRES-P as compared to CTRL-P, but the original and alternative formulations again perform equally well, whereas the gust formulation exhibits higher spatial RMSE (Table 3).

The parameterization also succeeds in reproducing the seasonal cycle of haboobs related to the monsoon over the Sahel west and east and the Sahara west. With the original formulation applied to CTRL-P, the parameterization captures the primary peak in June over the Sahel west (solid red curve in Figure 12e) and in August over the Sahara west and the Sahel east (solid red curves in Figures 12c and 12f). The parameterization also captures the weaker seasonal cycle over the Mediterranean and Sahara east areas (solid red curves in Figures 12b and 12d). In contrast, the parameterization poorly captures the seasonal cycle over the Atlas, where it overestimates the weak peak in February and underestimates the stronger peaks in May and July (solid red curve in Figure 12a). This suggests that the parameterization produces too high DUP in the convection embedded in winter storms and too low DUP in the convection favored by upper level troughs in spring and summer. The parameterization also overestimates the weak peak in February over the Mediterranean, Sahara west, and Sahel west areas (solid red curves in Figures 12b, 12c, and 12e).

As for the spatial distribution, applying the parameterization to HIRES-P instead of CTRL-P weakly impacts on the seasonal cycle, although the amplitude increases over the Sahel west and east (solid orange curves in Figures 12e and 12f). This is consistent with the higher amplitude of the monsoon cycle in HIRES-P (orange curves in Figures 5e and 5f). The higher amplitude of DUP increases the seasonal RMSE as compared to CTRL-P (Table 3). As for the spatial distribution again, using the alternative formulation weakly affects the seasonal cycle, although DUP slightly decreases in winter and increases in spring and summer (dashed curves in Figure 12). This improves the seasonal cycle and decreases the seasonal RMSE in CTRL-P and HIRES-P (Table 3).

In contrast with the alternative formulation, using the gust formulation strongly changes the seasonal cycle. After increasing during the monsoon onset, DUP stagnates over the Sahel east and even drops over the Sahel west (dotted curves in Figures 12e and 12f). This is due to the asymmetry in DCAPE between the monsoon onset and retreat, which matches the observed dust uplift over the Sahel and southern Sahara [Marshall *et al.*, 2008]. Over the Atlas area, the gust formulation reaches a peak in August (dotted curves in Figure 12a), which also matches the observed frequency of haboobs [Emmel *et al.*, 2010]. This, however, contrasts with the seasonal cycle of haboobs in EXPL (blue curves in Figures 12a, 12e, and 12f), which therefore suggests that the

match between the gust formulation and the observations is due to compensating errors. Finally, the weak peak in February vanishes with the gust formulation (dotted curves in Figure 12), which improves the seasonal cycle. The gust formulation still shows the highest seasonal RMSE for both CTRL-P and HIRES-P (Table 3).

The parameterization does not succeed in capturing the diurnal cycle of haboobs. With all formulations and applied to all runs, the parameterized DUP increases quicker in the morning and reaches its peak earlier in the afternoon as compared to EXPL (Figure 13). This is consistent with the parameterized convection reaching its peak at noon (Figure 6), which is a known issue in the Tropics [e.g., Marsham *et al.*, 2013b; Birch *et al.*, 2014]. The amplitude increases but the diurnal cycle is weakly impacted when using the alternative formulation (dashed curves in Figure 13). In contrast, the amplitude of the diurnal cycle strongly increases with the gust formulation (dotted curves). This shows that the DCAPE exhibits a stronger diurnal cycle than the downdraft mass flux, which again suggests that computing the DCAPE in the deep Saharan boundary layer overestimates the parameterized DUP. The relative amplitude of the different formulations is consistent between the different areas (see Figure S5 for the diurnal cycle of haboobs over each area).

When added to the DUP from the resolved model wind, the parameterized DUP overall improves the seasonal cycle in CTRL-P and HIRES-P (dashed curves in Figure 8) as compared to EXPL. However, this total DUP still exhibits substantial biases, which can be explained by several factors. On the one hand, the parameterization itself exhibits biases as compared to EXPL, e.g., the underestimation of DUP from haboobs over the Atlas in spring and summer (Figure 12a). The tuning of the parameterization may also contribute to the underestimation, as it uses the rather conservative identification of haboobs in EXPL as a reference. On the other hand, the resolution is expected to affect the resolved winds independently of haboobs, e.g., over complex topography, or for specific processes such as the low-level jet. The resolution furthermore leads to the overestimation of DUP from resolved winds over the Sahel west in summer, where the representation of the monsoon is affected (Figure 5e) and deep cyclones develop (Figure 10b) in CTRL-P and HIRES-P. The parameterization therefore offers a solution for the important issue of lacking haboobs in the model runs with parameterized convection, but other biases need to be carefully investigated in these model runs. Finally, the parameterized DUP improves the diurnal cycle in CTRL-P and HIRES-P (dashed curves in Figure 9) as compared to EXPL but through a general increase in DUP only.

5. Conclusion

Haboobs occur over most dust sources worldwide and contribute at least half of dust emissions over the central Sahara in summer [Marsham *et al.*, 2013a; Allen *et al.*, 2013, 2015]. However, they are absent from most large-scale weather and climate models, which do not explicitly represent convection and thus haboobs. Here an unprecedented 1 year long run with explicit convection delivers the first full seasonal cycle of haboobs over the different arid regions of northern Africa. This computationally very expensive run further allows testing a simple parameterization based on the downdraft mass flux of the convection scheme, originally developed in PKMB15, in a set of additional model runs with parameterized convection.

The explicit run exhibits two contrasting regimes. The highest DUP (dust uplift potential, i.e., dust-generating winds) from haboobs is found in the subtropical regime over the Atlas and northern Algeria, where it reaches its peak in spring and summer due to midlatitude troughs. High DUP from haboobs is also found in the tropical regime over the Sahel and the western Sahara, where it reaches its peak in summer due to the monsoon flow. The results are consistent with observations of haboobs during the few field campaigns over these areas, as well as with an earlier explicit run restricted to the western Sahel and Sahara and to a shorter time period. Low DUP from haboobs is finally found over the dry eastern Sahara. The contribution of haboobs to the total DUP reaches 18% annually over northern Africa, 24% between May and October, and up to 33% over the western Sahel during that period.

The parameterization succeeds in capturing the spatial pattern of DUP from haboobs as compared to the explicit run. The parameterization also succeeds in capturing the seasonal cycle due to the monsoon in the tropical regime, while it struggles with the seasonal cycle due to midlatitude systems in the subtropical regime. The parameterization can be tuned for the model resolution and for an alternative formulation with weak impact on the spatial and temporal distributions. In contrast, using a formulation based on DCAPE shifts the parameterized DUP northward and worsens the results. With the original and the alternative formulation, the parameterization improves the seasonal cycle of DUP, although the overall performance remains constrained by other limitations in the model runs.

The main limitations are common to both explicit and parameterized runs. The diurnal cycle of haboobs differs between parameterized and explicit DUP and also between explicit DUP from two different models, which is consistent with differences in the diurnal cycle of precipitation and emphasizes the uncertainty in modeling convective organization. The seasonal cycle in the subtropical regime contrasts between parameterized and explicit DUP from haboobs and also between explicit and observed DUP, which is again consistent with differences in the seasonal cycle of precipitation and suggests a model deficiency in this regime. Finally, the spatial distribution differs over the Sahel west between parameterized and explicit DUP from haboobs and also between modeled and observed DUP, which shows the high sensitivity to the roughness length in this area.

The results are also subject to uncertainties in the spatial and seasonal distribution of haboobs. One part of the uncertainty lies in the identification of haboobs in the explicit run, which becomes ambiguous when the cold pools evolve into complex structures [Heinold *et al.*, 2013], the identification being rather conservative here. The other part of the uncertainty lies in the scarcity of surface observations, which lack both spatial and temporal sampling over northern Africa [Cowie *et al.*, 2014]. Furthermore, identifying haboobs is challenging and must often be done manually, even with high-resolution data [Engerer *et al.*, 2008; Provod *et al.*, 2015]. This raises the need for more observations over northern Africa or for new algorithms to identify haboobs in available satellite and surface observations, as recently suggested by Redl *et al.* [2015].

Despite the limitations discussed above, the results presented here show that the parameterization originally developed by PKMB15 is robust with respect to the model and its resolution, as well as to the formulation with constant radius or constant propagation speed of cold pools. The parameterization is simple and can be used online or offline, providing that the downdraft mass flux is stored, in large-scale weather and climate models with mass flux convection schemes. It can thus be implemented in full dust models and the results be compared with extensive observations beyond the SYNOP winds considered here, as, e.g., aerosol optical depth (AOD) from satellites and Aerosol Robotic Network stations. The parameterization has the potential to solve a long-standing issue in simulating dust storms. In particular, it may compensate for the too low AOD over summertime West Africa in large-scale dust models compared to observations [e.g., Johnson *et al.*, 2011; Ridley *et al.*, 2012; Guirado *et al.*, 2014; Cuevas *et al.*, 2015]. It has potential to solve a long-standing issue in simulating dust storms.

Acknowledgments

The authors thank Vera Maurer for valuable discussions about the COSMO-CLM simulations and Sophie Cowie for guidance to use SYNOP observations, as well as two anonymous reviewers for constructive comments that helped in improving the manuscript. The authors gratefully acknowledge the computing time granted by the John von Neumann Institute for Computing (NIC) and provided on the supercomputer JUROPA at Jülich Supercomputing Centre (JSC). For access to the model data please contact ingeborg.bischoff-gauss@kit.edu. The TRMM data were obtained through the NASA Goddard Earth Sciences (GES) Data and Information Services Center (DISC). The SYNOP data were obtained through the Met Office Integrated Data Archive System (MIDAS). The code for parameterizing haboobs is available from the corresponding author upon request. This work was funded by the European Research Council (ERC) grant 257543 "Desert Storms."

References

- Allen, C. J., R. Washington, and S. Engelstaedter (2013), Dust emission and transport mechanisms in the central Sahara: Fennec ground-based observations from Bordj Badji Mokhtar, June 2011, *J. Geophys. Res. Atmos.*, *118*, 6212–6232, doi:10.1002/jgrd.50534.
- Allen, C. J. T., R. Washington, and A. Saci (2015), Dust detection from ground-based observations in the summer global dust maximum: Results from Fennec 2011 and 2012 and implications for modeling and field observations, *J. Geophys. Res. Atmos.*, *120*, 897–916, doi:10.1002/2014JD022655.
- Alpert, P., and B. Ziv (1989), The Sharav cyclone: Observations and some theoretical considerations, *J. Geophys. Res.*, *94*(D15), 18,495–18,514, doi:10.1029/JD094iD15p18495.
- Baldauf, M., A. Seifert, J. Förstner, D. Majewski, M. Raschendorfer, and T. Reinhardt (2011), Operational convective-scale numerical weather prediction with the COSMO model: Description and sensitivities, *Mon. Weather Rev.*, *139*(12), 3887–3905, doi:10.1175/MWR-D-10-05013.1.
- Berry, G., and C. Thorncroft (2005), Case study of an intense African easterly wave, *Mon. Weather Rev.*, *133*(4), 752–766, doi:10.1175/MWR2884.1.
- Birch, C. E., D. J. Parker, J. H. Marsham, D. Copsey, and L. Garcia-Carreras (2014), A seamless assessment of the role of convection in the water cycle of the West African monsoon, *J. Geophys. Res. Atmos.*, *119*, 2890–2912, doi:10.1002/2013JD020887.
- Bou Karam, D., C. Flamant, P. Knippertz, O. Reitebuch, J. Pelon, M. Chong, and A. Dabas (2008), Dust emissions over the Sahel associated with the West African monsoon intertropical discontinuity region: A representative case-study, *Q. J. R. Meteorol. Soc.*, *134*(632), 621–634, doi:10.1002/qj.244.
- Cowie, S. M., P. Knippertz, and J. H. Marsham (2014), A climatology of dust emission events from northern Africa using long-term surface observations, *Atmos. Chem. Phys.*, *14*(16), 8579–8597, doi:10.5194/acp-14-8579-2014.
- Cuevas, E., *et al.* (2015), The MACC-II 2007–2008 reanalysis: Atmospheric dust evaluation and characterization over northern Africa and the Middle East, *Atmos. Chem. Phys.*, *15*(8), 3991–4024, doi:10.5194/acp-15-3991-2015.
- Dee, D. P., *et al.* (2011), The ERA-Interim reanalysis: Configuration and performance of the data assimilation system, *Q. J. R. Meteorol. Soc.*, *137*(656), 553–597, doi:10.1002/qj.828.
- Emmel, C., P. Knippertz, and O. Schulz (2010), Climatology of convective density currents in the southern foothills of the Atlas Mountains, *J. Geophys. Res.*, *115*, D11115, doi:10.1029/2009JD012863.
- Engerer, N. A., D. J. Stensrud, and M. C. Coniglio (2008), Surface characteristics of observed cold pools, *Mon. Weather Rev.*, *136*(12), 4839–4849, doi:10.1175/2008MWR2528.1.
- Fiedler, S., K. Schepanski, B. Heinold, P. Knippertz, and I. Tegen (2013), Climatology of nocturnal low-level jets over North Africa and implications for modeling mineral dust emission, *J. Geophys. Res. Atmos.*, *118*, 6100–6121, doi:10.1002/jgrd.50394.
- Fink, A. H., and A. Reiner (2003), Spatiotemporal variability of the relation between African easterly waves and West African squall lines in 1998 and 1999, *J. Geophys. Res.*, *108*(D11), 4332–4348, doi:10.1029/2002JD002816.

- Flamant, C., J.-P. Chaboureaud, D. J. Parker, C. M. Taylor, J.-P. Cammas, O. Bock, F. Timouk, and J. Pelon (2007), Airborne observations of the impact of a convective system on the planetary boundary layer thermodynamics and aerosol distribution in the inter-tropical discontinuity region of the West African monsoon, *Q. J. R. Meteorol. Soc.*, **133**(626), 1175–1189, doi:10.1002/qj.97.
- Fujita, T., and H. Byers (1977), Spearhead echo and downburst in crash of an airliner, *Mon. Weather Rev.*, **105**(2), 129–146, doi:10.1175/1520-0493(1977)105<0129:SEADIT>2.0.CO;2.
- Gantner, L., and N. Kalthoff (2010), Sensitivity of a modelled life cycle of a mesoscale convective system to soil conditions over West Africa, *Q. J. R. Meteorol. Soc.*, **136**(51), 471–482, doi:10.1002/qj.425.
- Garcia-Carreras, L., J. Marsham, D. Parker, C. Bain, S. Milton, A. Saci, M. Salah-Ferroudj, B. Ouchene, and R. Washington (2013), The impact of convective cold pool outflows on model biases in the Sahara, *Geophys. Res. Lett.*, **40**, 1647–1652, doi:10.1002/grl.50239.
- Grandpeix, J.-Y., and J.-P. Lafore (2010), A density current parameterization coupled with Emanuel's convection scheme. Part I: The models, *J. Atmos. Sci.*, **67**(4), 881–897, doi:10.1175/2009JAS3044.1.
- Guirado, C., et al. (2014), Aerosol characterization at the Saharan AERONET site Tamanrasset, *Atmos. Chem. Phys.*, **14**(21), 11,753–11,773, doi:10.5194/acp-14-11753-2014.
- Heinold, B., P. Knippertz, J. Marsham, S. Fiedler, N. Dixon, K. Schepanski, B. Laurent, and I. Tegen (2013), The role of deep convection and nocturnal low-level jets for dust emission in summertime West Africa: Estimates from convection-permitting simulations, *J. Geophys. Res. Atmos.*, **118**, 4385–4400, doi:10.1002/jgrd.50402.
- Heise, E. (2006), Improved diagnosis of convective and turbulent gusts: Test results of new gust parameterization, *COSMO Newslett.*, **6**, 103–114.
- Houze, R. A. (2004), Mesoscale convective systems, *Rev. Geophys.*, **42**, RG4003, doi:10.1029/2004RG000150.
- Huffman, G. J., D. T. Bolvin, E. J. Nelkin, D. B. Wolff, R. F. Adler, G. Gu, Y. Hong, K. P. Bowman, and E. F. Stocker (2007), The TRMM Multisatellite Precipitation Analysis (TMPA): Quasi-global, multiyear, combined-sensor precipitation estimates at fine scales, *J. Hydrometeorol.*, **8**(1), 38–55, doi:10.1175/JHM560.1.
- Johnson, B. T., M. E. Brooks, D. Walters, S. Woodward, S. Christopher, and K. Schepanski (2011), Assessment of the Met Office dust forecast model using observations from the GERBILS campaign, *Q. J. R. Meteorol. Soc.*, **137**(658), 1131–1148, doi:10.1002/qj.736.
- Knippertz, P. (2003), Tropical-extratropical interactions causing precipitation in Northwest Africa: Statistical analysis and seasonal variations, *Mon. Weather Rev.*, **131**(12), 3069–3076, doi:10.1175/1520-0493(2003)131<3069:TICPIN>2.0.CO;2.
- Knippertz, P. (2014), Meteorological aspects of dust storms, in *Mineral Dust*, edited by P. Knippertz, pp. 121–147, Springer, Netherlands., doi:10.1007/978-94-017-8978-3
- Knippertz, P., A. H. Fink, A. Reiner, and P. Speth (2003), Three late summer/early autumn cases of tropical-extratropical interactions causing precipitation in Northwest Africa, *Mon. Weather Rev.*, **131**(1), 116–135, doi:10.1175/1520-0493(2003)131<0116:TLSEAC>2.0.CO;2.
- Knippertz, P., C. Deutscher, K. Kandler, T. Müller, O. Schulz, and L. Schütz (2007), Dust mobilization due to density currents in the Atlas region: Observations from the Saharan Mineral Dust Experiment 2006 field campaign, *J. Geophys. Res.*, **112**, D21109, doi:10.1029/2007JD008774.
- Knippertz, P., J. Trentmann, and A. Seifert (2009), High-resolution simulations of convective cold pools over the northwestern Sahara, *J. Geophys. Res.*, **114**, D08110, doi:10.1029/2008JD011271.
- Kocha, C., P. Tulet, J.-P. Lafore, and C. Flamant (2013), The importance of the diurnal cycle of aerosol optical depth in West Africa, *Geophys. Res. Lett.*, **40**, 785–790, doi:10.1002/grl.50143.
- Laing, A. G., R. Carbone, V. Levizzani, and J. Tuttle (2008), The propagation and diurnal cycles of deep convection in northern tropical Africa, *Q. J. R. Meteorol. Soc.*, **134**(630), 93–109, doi:10.1002/qj.194.
- Largerou, Y., F. Guichard, D. Bouniol, F. Couvreux, L. Kergoat, and B. Marticorena (2015), Can we use surface wind fields from meteorological reanalyses for Sahelian dust emission simulations?, *Geophys. Res. Lett.*, **42**, 2490–2499, doi:10.1002/2014GL062938.
- Marsham, J. H., D. J. Parker, C. M. Grams, C. M. Taylor, and J. M. Haywood (2008), Uplift of Saharan dust south of the intertropical discontinuity, *J. Geophys. Res.*, **113**, D21102, doi:10.1029/2008JD009844.
- Marsham, J. H., C. M. Grams, and B. Mühr (2009), Photographs of dust uplift from small-scale atmospheric features, *Weather*, **64**(7), 180–181, doi:10.1002/wea.390.
- Marsham, J. H., P. Knippertz, N. S. Dixon, D. J. Parker, and G. M. S. Lister (2011), The importance of the representation of deep convection for modeled dust-generating winds over West Africa during summer, *Geophys. Res. Lett.*, **38**, L16803, doi:10.1029/2011GL048368.
- Marsham, J. H., et al. (2013a), Meteorology and dust in the central Sahara: Observations from Fennec supersite-1 during the June 2011 Intensive Observation Period, *J. Geophys. Res. Atmos.*, **118**, 4069–4089, doi:10.1002/jgrd.50211.
- Marsham, J. H., N. S. Dixon, L. Garcia-Carreras, G. Lister, D. J. Parker, P. Knippertz, and C. E. Birch (2013b), The role of moist convection in the West African monsoon system: Insights from continental-scale convection-permitting simulations, *Geophys. Res. Lett.*, **40**, 1843–1849, doi:10.1002/grl.50347.
- Marticorena, B., and G. Bergametti (1995), Modeling the atmospheric dust cycle: 1. Design of a soil-derived dust emission scheme, *J. Geophys. Res.*, **100**(D8), 16,415–16,430, doi:10.1029/95JD00690.
- Marticorena, B., B. Chatenet, J.-L. Rajot, S. Traoré, M. Coulibaly, A. Diallo, I. Koné, A. Maman, T. NDiaye, and A. Zakou (2010), Temporal variability of mineral dust concentrations over West Africa: Analyses of a pluriannual monitoring from the AMMA Sahelian Dust Transect, *Atmos. Chem. Phys.*, **10**(18), 8899–8915, doi:10.5194/acp-10-8899-2010.
- Nakamura, K., R. Kershaw, and N. Gait (1996), Prediction of near-surface gusts generated by deep convection, *Meteorol. Appl.*, **3**(2), 157–167, doi:10.1002/met.5060030206.
- O'Hara, S. L., M. L. Clarke, and M. S. Elatrash (2006), Field measurements of desert dust deposition in Libya, *Atmos. Environ.*, **40**(21), 3881–3897, doi:10.1016/j.atmosenv.2006.02.020.
- Panitz, H.-J., A. Dosio, M. Büchner, D. Lüthi, and K. Keuler (2014), COSMO-CLM (CCLM) climate simulations over CORDEX-Africa domain: Analysis of the ERA-Interim driven simulations at 0.44° and 0.22° resolution, *Clim. Dyn.*, **42**(11–12), 3015–3038, doi:10.1007/s00382-013-1834-5.
- Pantillon, F., P. Knippertz, J. H. Marsham, and C. E. Birch (2015), A parameterization of convective dust storms for models with mass-flux convection schemes, *J. Atmos. Sci.*, **72**(6), 2545–2561, doi:10.1175/JAS-D-14-0341.1.
- Parker, D., R. Burton, A. Diongue-Niang, R. Ellis, M. Felton, C. Taylor, C. Thorncroft, P. Bessemoulin, and A. Tompkins (2005), The diurnal cycle of the West African monsoon circulation, *Q. J. R. Meteorol. Soc.*, **131**, 2839–2860, doi:10.1256/qj.04.52.
- Provod, M., J. Marsham, D. Parker, and C. Birch (2015), A characterization of cold pools in the West African Sahel, *Mon. Weather Rev.*, doi:10.1175/MWR-D-15-0023.1, in press.
- Redl, R., A. H. Fink, and P. Knippertz (2015), An objective detection method for convective cold pool events and its application to northern Africa, *Mon. Weather Rev.*, **143**(12), 5055–5072, doi:10.1175/MWR-D-15-0223.1.
- Ridley, D. A., C. L. Heald, and B. Ford (2012), North African dust export and deposition: A satellite and model perspective, *J. Geophys. Res.*, **117**, D02202, doi:10.1029/2011JD016794.

- Ridley, D. A., C. L. Heald, J. Pierce, and M. Evans (2013), Toward resolution-independent dust emissions in global models: Impacts on the seasonal and spatial distribution of dust, *Geophys. Res. Lett.*, *40*, 2873–2877, doi:10.1002/grl.50409.
- Roberts, A. J., and P. Knippertz (2014), The formation of a large summertime Saharan dust plume: Convective and synoptic-scale analysis, *J. Geophys. Res. Atmos.*, *119*, 1766–1785, doi:10.1002/2013JD020667.
- Schepanski, K., and P. Knippertz (2011), Soudano-Saharan depressions and their importance for precipitation and dust: A new perspective on a classical synoptic concept, *Q. J. R. Meteorol. Soc.*, *137*(659), 1431–1445, doi:10.1002/qj.850.
- Schulz, J.-P., and E. Heise (2003), A new scheme for diagnosing near-surface convective gusts, *COSMO Newslett.*, *3*, 221–225.
- Sodemann, H., T. M. Lai, F. Marengo, C. L. Ryder, C. Flamant, P. Knippertz, P. Rosenberg, M. Bart, and J. B. McQuaid (2015), Lagrangian dust model simulations for a case of moist convective dust emission and transport in the western Sahara region during Fennec/LADUNEX, *J. Geophys. Res. Atmos.*, *120*, 6117–6144, doi:10.1002/2015JD023283.
- Sutton, L. J. (1925), Haboobs, *Q. J. R. Meteorol. Soc.*, *51*(213), 25–30, doi:10.1002/qj.49705121305.
- Tiedtke, M. (1989), A comprehensive mass flux scheme for cumulus parameterization in large-scale models, *Mon. Weather Rev.*, *117*(8), 1779, doi:10.1175/1520-0493(1989)117<1779:ACMFSF>2.0.CO;2.
- Todd, M., et al. (2013), Meteorological and dust aerosol conditions over the western Saharan region observed at Fennec Supersite-2 during the intensive observation period in June 2011, *J. Geophys. Res. Atmos.*, *118*, 8426–8447, doi:10.1002/jgrd.50470.
- Walters, D. N., et al. (2011), The Met Office Unified Model Global Atmosphere 3.0/3.1 and JULES Global Land 3.0/3.1 configurations, *Geosci. Model Dev.*, *4*(4), 919–941, doi:10.5194/gmd-4-919-2011.
- Washington, R., and M. C. Todd (2005), Atmospheric controls on mineral dust emission from the Bodélé Depression, Chad: The role of the low level jet, *Geophys. Res. Lett.*, *32*, L17701, doi:10.1029/2005GL023597.